Structural and functional analysis of Nro1/Ett1: a protein involved in translation termination in S. cerevisiae and in O2-mediated gene control in S. pombe

Delphine Rispal, Julien Henri, Herman van Tilbeurgh, Marc Graille, B Seraphin

Structural and functional analysis of Nro1/Ett1: a protein involved in translation termination in *S. cerevisiae* and in O_2-mediated gene control in *S. pombe*

DELPHINE RISPAL,[1,2,4] JULIEN HENRI,[3,4] HERMAN VAN TILBEURGH,[3] MARC GRAILLE,[3,5] and BERTRAND SÉRAPHIN[1,2,5]

[1]Equipe Labellisée La Ligue, Institut de Génétique et de Biologie Moléculaire et Cellulaire (IGBMC), CNRS UMR7104, Inserm U964, and Université de Strasbourg, Strasbourg, Illkirch F-67000, France
[2]Centre de Génétique Moléculaire (CGM), CNRS, F-91198 Gif-sur-Yvette Cedex, France
[3]Equipe "Fonction et Architecture des Assemblages Macromoléculaires", IBBMC (Institut de Biochimie et Biophysique Moléculaire et Cellulaire), CNRS, UMR8619, Bat 430, Université Paris Sud, F-91405 Orsay Cedex, France

ABSTRACT

In *Saccharomyces cerevisiae*, the putative 2-OG-Fe(II) dioxygenase Tpa1 and its partner Ett1 have been shown to impact mRNA decay and translation. Hence, inactivation of these factors was shown to influence stop codon read-though. In addition, Tpa1 represses, by an unknown mechanism, genes regulated by Hap1, a transcription factor involved in the response to levels of heme and O_2. The *Schizosaccharomyces pombe* orthologs of Tpa1 and Ett1, Ofd1, and its partner Nro1, respectively, have been shown to regulate the stability of the Sre1 transcription factor in response to oxygen levels. To gain insight into the function of Nro1/Ett1, we have solved the crystal structure of the *S. pombe* Nro1 protein deleted of its 54 N-terminal residues. Nro1 unexpectedly adopts a Tetratrico Peptide Repeat (TPR) fold, a motif often responsible for protein or peptide binding. Two ligands, a sulfate ion and an unknown molecule, interact with a cluster of highly conserved amino acids on the protein surface. Mutation of these residues demonstrates that these ligand binding sites are essential for Ett1 function in *S. cerevisiae*, as investigated by assaying for efficient translation termination.

Keywords: Tetratrico Peptide Repeats; translation termination; protein stability; crystal structure; read-through

INTRODUCTION

Protein synthesis is a major step of gene expression and relies on an intricate process that involves the synergistic action of mRNA, ribosomes, translation factors, and aminoacyl-tRNAs. The mechanism of translation proceeds in four successive and highly regulated operations: initiation, elongation, termination, and ribosome recycling. The fidelity during the transfer of genetic information from mRNAs to proteins relies, among others, on the high accuracy of the mRNA decoding process (elongation and termination) as well as on RNA quality control pathways (Doma and Parker 2007). Interestingly, in eukaryotes, several of these mechanisms involve at least two extrinsic and interacting factors (including a translational GTPase) that join the ribosome. During elongation, an aminoacyl-tRNA associated to the eEF-1A elongation factor with GTPase activity recognizes specifically its cognate codon present in the ribosomal A-site and thereby promotes peptidyl transfer (Taylor et al. 2007). When a stop codon is present in the ribosomal A site, a complex of two release factor proteins join the ribosome instead. The class I release factor eRF1 mimics a tRNA and directly recognizes the stop codon via a strongly conserved NIKS motif (Song et al. 2000; Frolova et al. 2002), while its associated class II release factor eRF3 displays sequence similarity with eEF-1A and harbors GTPase activity (Zhouravleva et al. 1995; Song et al. 2000; Kong et al. 2004). Binding of this complex to ribosomes triggers the release of the complete polypeptide through the action of a universally conserved GGQ motif from eRF1 and the dissociation of ribosomal subunits (Frolova et al. 1999; Alkalaeva et al. 2006). Structural analyses have demonstrated that the shapes of the tRNA-elongation factor complex and of release factors are very similar (Nissen et al. 1995; Cheng et al. 2009).

[4]These authors contributed equally this work.
[5]**Corresponding authors.**
E-mail marc.graille@u-psud.fr.
E-mail seraphin@igbmc.fr.
Article published online ahead of print. Article and publication date are at http://www.rnajournal.org/cgi/doi/10.1261/rna.2697111.

Recently, a third structurally related complex was described in archaea and eukaryotes (Chen et al. 2010; Kobayashi et al. 2010; van den Elzen et al. 2010). It is composed of two protein subunits, Dom34 and Hbs1, which are a tRNA mimic and a GTPase related to eEF-1A, respectively (Carr-Schmid et al. 2002; Graille et al. 2008). This complex was shown in yeast to target ribosomes accidentally stalled due to mRNA damage or a default in the small ribosomal subunit. Dom34/Hbs1 promotes the degradation of the defective RNA molecules (Doma and Parker 2006; Cole et al. 2009; Kobayashi et al. 2010; van den Elzen et al. 2010) and dissociation of the stalled ribosome with release of a peptidyl tRNA (Shoemaker et al. 2010).

The function of these protein assemblies mimicking a tRNA-elongation factor complex is best understood in the case of translation termination. This step depends on the specific and rapid recognition of stop codons by eRF1 despite the existence of near-cognate tRNAs (such as the $tRNA^{Trp}$) that could induce amino acid misincorporation and thereby production of longer proteins. In eukaryotes, the efficiency of stop codon recognition is primarily influenced by the stop codon itself and the first downstream nucleotide (Bonetti et al. 1995). In addition, several proteins such as Pab1, Rli1, Npl3, Gle1, and Dbp5, as well as the inositol hexakisphosphate IP6 molecule act as *trans*-acting factors, at least in yeast *Saccharomyces cerevisiae* (Cosson et al. 2002; Gross et al. 2007; Bolger et al. 2008; Estrella et al. 2009; Alcazar-Roman et al. 2010; Khoshnevis et al. 2010). These factors may influence translation termination efficiency through the release factors eRF1 and eRF3, which they have been described to interact with.

Tpa1 is another protein that was implicated in modulating translation termination efficiency in *S. cerevisiae* by reducing stop-codon read-through (Keeling et al. 2006; Henri et al. 2010). In addition, this protein was shown to interact with Pab1, eRF1, and eRF3 and hence proposed to be part of an mRNP complex associated at the mRNA 3′ end (Keeling et al. 2006). Structure and sequence analysis strongly support that Tpa1 belongs to the 2-oxoglutarate-Fe(II) dioxygenase family and most probably acts as a prolyl hydroxylase (PHD), an enzyme catalyzing the O_2-dependant hydroxylation of the proline side-chain (Henri et al. 2010; Kim et al. 2010). However, this catalytic activity remains experimentally elusive, most likely because a biologically relevant substrate has not yet been identified. Tpa1 is composed of a N-terminal putative PHD domain harboring the **HXD**...**H** signature found in this family of proteins and a C-terminal domain devoid of catalytic residues. We have shown that the two Tpa1 domains, as well as the integrity of Tpa1 putative active site, are required for efficient translation termination (Henri et al. 2010). In addition, Tpa1 contributes to the repression of genes regulated by Hap1, a transcription factor involved in the response to levels of heme and oxygen (Henri et al. 2010), raising the possibility that it may influence translation termination by affecting eRF1 protein levels. However, we were not able to detect any differences in eRF1 levels in *tpa1Δ* cells compared with wild-type cells (D Rispal and B Séraphin, unpubl.). In parallel, a Tpa1 ortholog from *Schizosaccharomyces pombe*, Ofd1, has been implicated in the O_2-dependent regulation of the stability of the Sre1 transcription factor that regulates the expression of genes involved in cholesterol and lipid biosynthesis (Hughes and Espenshade 2008). In this case, the integrity of the Ofd1 putative PHD active site seems not to be required for Sre1 degradation but rather to modulate oxygen sensing (Hughes and Espenshade 2008). Under low oxygen levels, the membrane bound Sre1 protein is proteolytically cleaved, thus releasing its N-terminal domain ($Sre1_N$) that enters the nucleus and activates the expression of genes essential for hypoxic growth (Hughes et al. 2005, 2007; Todd et al. 2006). In the presence of oxygen, Ofd1 acts as a sensor and enhances the degradation of $Sre1_N$ (Hughes and Espenshade 2008). A genetic screen identified *S. pombe* Nro1, a poorly characterized protein, as a negative regulator of Ofd1 (Chen et al. 2004; Lee et al. 2009). Detailed characterization of the mechanisms involved suggests that under normoxia, the Ofd1 N-terminal dioxygenase domain prevents binding of Nro1 to the Ofd1 C-terminal domain; thus, the latter is free to accelerate the degradation of $Sre1_N$. In contrast, under hypoxia, the Ofd1 dioxygenase domain is inactive, allowing Nro1 to bind to the Ofd1 C-terminal domain, thus preventing the latter to destabilize the $Sre1_N$ domain.

Interestingly, the *S. cerevisiae YOR051C* open reading frame encodes a Nro1 ortholog that has been shown to interact with Tpa1 by high-throughput tandem-affinity purification (Krogan et al. 2006). Moreover, this protein and Tpa1 copurify with the yeast nuclear pore complex (Rout et al. 2000), suggesting that they could be involved in mRNA export similarly to Dbp5, Npl3, and Gle1, which also influence translation termination efficiency (Gross et al. 2007; Bolger et al. 2008; Estrella et al. 2009). However, deletion of either *TPA1* or *NRO1* genes does not affect mRNA export in budding and fission yeasts, respectively, making this possibility unlikely (Chen et al. 2004; Keeling et al. 2006). The *YOR051C* encoded protein also inhibits the replication of Brome mosaic virus in *S. cerevisiae* similarly to genes coding for proteins involved in mRNA metabolism (Ski complex and Ski7) (Kushner et al. 2003). Finally, this protein copurifies with ribosomal proteins together with Stm1 (Van Dyke et al. 2004), a protein modulating mRNA decay (Balagopal and Parker 2009) and involved in TOR signaling. Based on the established links between *YOR051C* and Tpa1 and between their homologs Ofd1 and Nro1 in *S. pombe*, as well as on the effect of Tpa1 on translation termination efficiency, we have previously tested the effect of *YOR051C* deletion on stop codon read-through in *S. cerevisiae* and observed a similar, albeit weaker, phenotype as *TPA1* gene deletion (i.e., a significant increase of stop-codon read-through). Thus, we named the gene product Ett1 (for Enhancer of translation

termination 1) (Henri et al. 2010). Contrary to the inhibitory effect of Nro1 on Ofd1 in *S. pombe*, the effect of *ETT1* deletion is comparable to that of *TPA1* deletion. Moreover, Ett1 and Tpa1 inactivation are not additive, arguing that both proteins act in the same pathway and that Ett1 does not inhibit Tpa1. Altogether, these studies establish a functional link between Tpa1 and Ett1 in *S. cerevisiae* similar to the one observed between Ofd1 and Nro1 in *S. pombe*. However, it remains to be established how these orthologous proteins are involved in these two different pathways that have been described in two different species. To gain a mechanistic insight into Nro1/Ett1 function, we have solved the crystal structure of a fragment from *S. pombe* Nro1. This served as the starting point for a structure-based functional study in vivo in yeast *S. cerevisiae*.

RESULTS AND DISCUSSION

Nro1 structure resolution

To obtain structural information on Ett1/Nro1, we prepared various constructs to overexpress these factors in *Escherichia coli*. As the Ett1 protein from *S. cerevisiae* proved to be poorly stable in all conditions tested (data not shown), we focused our efforts on Nro1, its ortholog from *S. pombe*. Good expression and crystals were obtained for an Nro1 construct lacking its first 54 N-terminal residues that were predicted to be poorly folded by bioinformatics analysis (hereafter named $Nro1_{\Delta N54}$). We solved the structure of this protein using the multi-wavelength anomalous diffusion (MAD) method from SeMet substituted protein crystals. The protein crystallized in two different space groups ($P2_1$ and $P6_522$), and the corresponding structures showed no significant difference after complete rebuilding and refinement (root mean square deviation [rmsd] = 0.55 Å over 322 aligned residues).

The model obtained from the highest-resolution data set ($P2_1$) contained two copies in the asymmetric unit that are virtually identical (rmsd = 0.35 Å). These two molecules interact via a large surface of 2250 $Å^2$, raising the possibility that this protein associates as a homodimer. However, a size-exclusion chromatography coupled to a multi-angle laser light scattering (MALLS) experiment yielded a molecular weight of 39.7 kDa, very close to the theoretical value expected for a monomer (39.5 kDa) (data not shown). We thus conclude that $Nro1_{\Delta N54}$ is monomeric in solution and that the observed dimer is more likely imposed by crystal packing forces.

Nro1 belongs to the Tetratrico Peptide Repeat superfamily

The $Nro1_{\Delta N54}$ monomer is composed of six pairs of antiparallel helices and a short C-terminal amphipathic helix (hC) stacked onto the last helical hairpin motif (Fig. 1A).

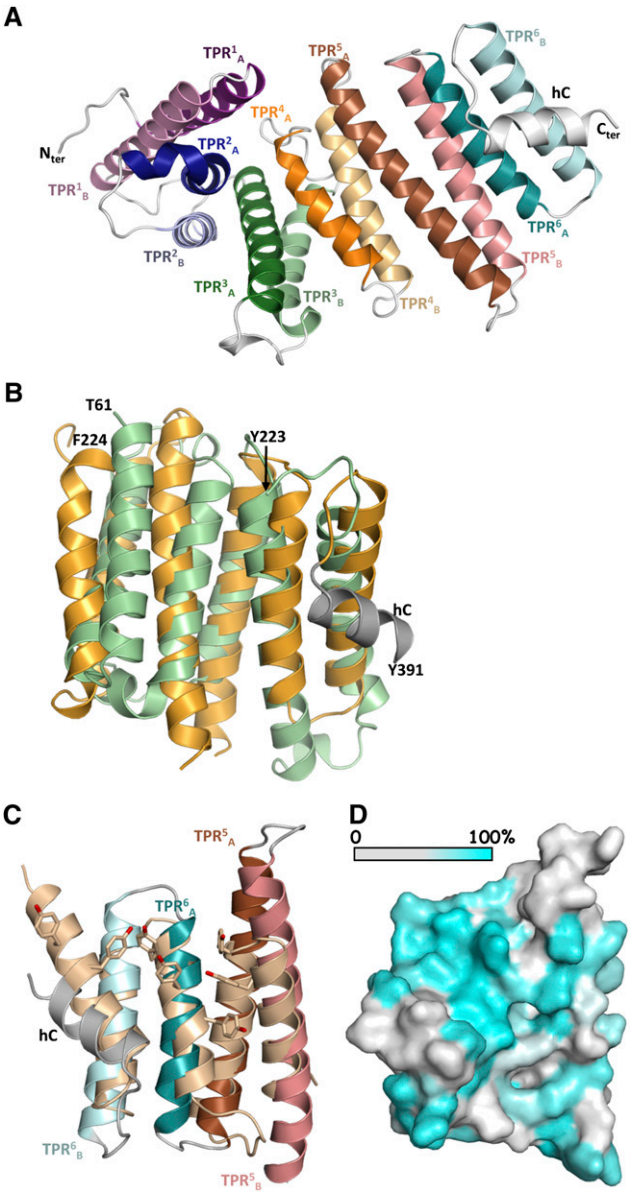

FIGURE 1. $Nro1_{\Delta N54}$ structure. (*A*) Ribbon representation of the $Nro1_{\Delta N54}$ monomer. Each TPR unit is represented with different colors. Helices A and B are in dark and light colors, respectively. (*B*) Superposition of the Nro1-C domain (light green) onto the Nro1-N domain (orange). (*C*) Ribbon representation of the superimposition of the C-P4H TPR domain (beige) onto the Nro1-C domain (same color-code as panel *A*). The Tyr side-chains from C-P4H TPR domains that have been shown to be involved in substrate binding are depicted as sticks. (*D*) Mapping of the residue conservation at the surface of Nro1-C domain. Color-coding is from white (no conservation) to cyan (high conservation). To facilitate the comparison, the same scale of sequence conservation has been used in all the figures. The orientation is similar to panel *C*. For clarity, the C-P4H TPR domain has been omitted.

The hydrophobic face of helix hC packs onto a hydrophobic patch on the preceding helix pair, while its polar face is exposed to the solvent, allowing helix hC to act as a solvating cap that stabilizes the Nro1 protein. The packing of helical

pairs creates a right-handed superhelical arrangement, as observed for other members of the Tetratrico Peptide Repeat (TPR) superfamily. Hence, based on its structure, Nro1 can be considered as a new member of this TPR family that includes bacterial and eukaryotic proteins. Such structural classification was not predicted earlier by classical bioinformatics tools used to analyze the entire protein sequence.

TPR proteins are composed of three to 16 tandem peptide repeat motifs of 34 amino acids with degenerate sequence. The helical pairs adopt a helix-turn-helix anti-parallel arrangement with interacting helices (i.e., helix A and helix B) separated by a short loop (D'Andrea and Regan 2003). In general, TPR motifs are stacked together so that helix A from TPR^n is packed between helix B from TPR^n and helix A from TPR^{n+1}. In Nro1, the 12 α helices forming the six TPR motifs are organized as follows from N terminus to C terminus: TPR^1_A, TPR^1_B, TPR^2_A, TPR^2_B, TPR^3_A, TPR^3_B, TPR^4_A, TPR^4_B, TPR^5_A, TPR^5_B, TPR^6_A, and TPR^6_B with the C-terminal helix (hC) running above the sixth TPR motif with an angle of ~45° with TPR^6_A and TPR^6_B (Figs. 1A, 2). The corresponding TPRs structural motifs are longer (50 residues) than are canonical ones (34 amino acids) and are organized into two subdomains: Nro1-N (residues 55–225) and Nro1-C (residues 226–393). Nro1-N is composed of TPR^1 to TPR^3 motifs, and within this domain, consecutive TPR units are related by a 34° rotation. Nro1-C is formed by TPR^4 to TPR^6 motifs, and in this case, consecutive TPR units are related by a rotation of 15°. These Nro1-N and Nro1-C subdomains are similar in structure (rmsd of 2.8 Å over 97 Cα atoms; 10% sequence identity) (Fig. 1B). The C-terminal TPR unit from Nro1-N (TPR^3) and the N-terminal TPR from Nro1-C (TPR^4) are related by a rotation of 50°. Hence, Nro1 does not form a highly regular right-handed helix compared to, for instance, *S. cerevisiae* Sec17, a TPR protein involved in vesicular transport (Rice and Brunger 1999).

Because the structure of Nro1 revealed an assembly of noncanonical TPR motifs, we analyzed the sequence of *S. pombe* Nro1 using the bioinformatics tool TPRPred (MPI Tübingen, http://toolkit.tuebingen.mpg.de/tprpred) designed for the prediction of TPR motifs. This server indeed predicted the six TPR motifs observed in the structure from each motif sequence. Another TPR motif (TPR^0) is predicted between Arg^5 and Pro^{38}, a region deleted in the Nro1 fragment used in this study. Full-length Nro1 very likely contains seven divergent TPR modules plus the C-ter capping helix (hC). This architecture is not uncommon since 20% of the TPR-containing proteins in *S. cerevisiae* are predicted to contain seven repeats (D'Andrea and Regan 2003).

Comparison with other TPR proteins

TPR proteins are ubiquitous and frequently engaged in protein–protein or protein–peptide interactions effecting different functions: for example, transcriptional regulation, protein translocation, cell cycle control, pre-mRNA splicing, and peptidyl prolyl isomerase (D'Andrea and Regan 2003). Numerous structures of TPR proteins have already been described, and they commonly bind peptides within their concave groove. This is, for instance, the case for cochaperone proteins such as cyclophilin 40 (Cyp40), the Hsp70/Hsp90 organizing protein (Hop), and FK506 binding proteins (FKBPs), which all bind the acidic C-terminal MEEVD peptide from Hsp90 (Riggs et al. 2003; Wu et al. 2004).

A search for proteins sharing structural similarity with $Nro1_{\Delta N54}$ using the DALI server (Holm et al. 2008) identified approximately 100 proteins with *Z*-scores ranging from 12 to 5. However, with the exception of the bacterial PilF protein from *Pseudomonas aeruginosa* (rmsd of 4.1 Å over 200 Cα atoms; 8% sequence identity) (Kim et al. 2006), these proteins display high rmsd values compared with the entire crystallized Nro1 fragment (rmsd of 7–9 Å for structural alignment of 200–230 residues). Since the structure of Nro1 can be divided into two domains (Nro1-N and Nro1-C), we have searched the structure database for the subdomains separately. Strikingly, the same strong structural similarities are found for both the Nro1-N and Nro1-C domains (*Z*-scores of 9–11 and rmsd ranging from 2.5–4 Å over 90–120 Cα atoms; sequence identity between 5% and 14%). Among those, one is of particular interest in light of the implication of Nro1/Ett1 in the pathways involving putative prolyl-4-hydroxylases Ofd1/Tpa1 (Lee et al. 2009; Henri et al. 2010).

Indeed, the TPR domain from the α subunit of human collagen prolyl-4-hydroxylase (C-P4H) $\alpha_2\beta_2$ tetramer displays rmsd values of 2.9 Å over 90 Cα atoms (5% sequence identity) and 2.7 Å over 81 Cα atoms (5% sequence identity) with the Nro1-N and Nro1-C domains, respectively (Fig. 1C; Pekkala et al. 2004). The C-P4H TPR domain is involved in the binding of the $[X\text{-}Pro\text{-}Gly]_n$ triplets from collagen and enhances the activity of the C-P4H catalytic dioxygenase domain (also located within this α subunit) responsible for hydroxylation of the Pro side-chains from collagen. This domain has a higher affinity for peptides containing unmodified Pro side-chains than for peptides containing hydroxylated Pro (Hyp) (Hieta et al. 2003). Its peptide-binding site is located in the concave surface formed by helices A from contiguous TPR units and is lined by several Tyr side-chains important for peptide binding. Equivalent Tyr side-chains are not present in Nro1 orthologs, but the region corresponding to this peptide binding groove in Nro1-C is one of the most-conserved region within Nro1/Ett1 family (Fig. 1D). Although the prolyl-4-hydroxylase activity of Tpa1/Ofd1 remains to be demonstrated, we hypothesized that Nro1/Ett1 assists it in substrate recruitment. Nro1 from *S. pombe* has been shown to interact physically with the Ofd1 C-terminal domain, but this interaction is likely to be transient, as a reversible cross-linker was needed to stabilize binding. This interaction is also strengthened by

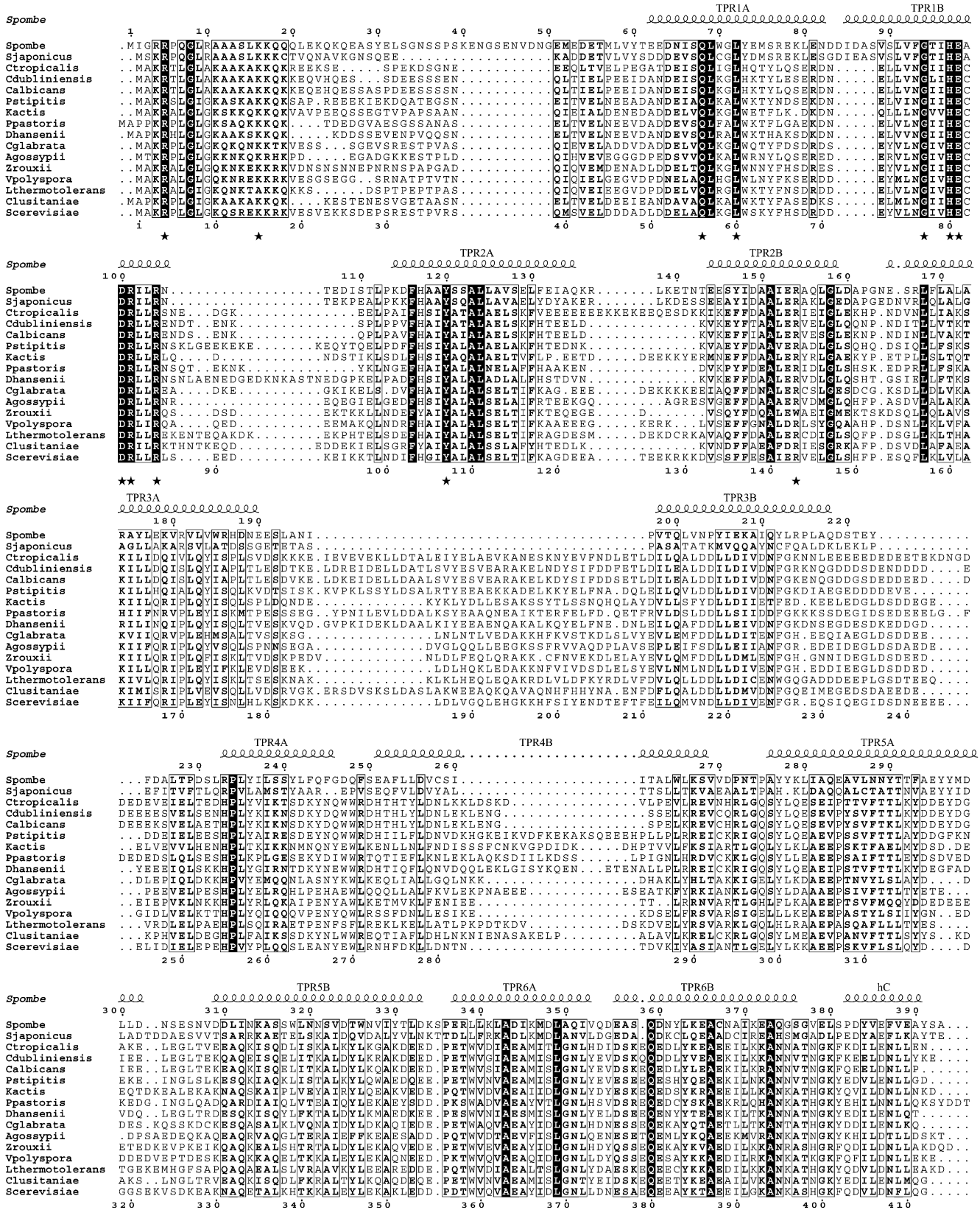

FIGURE 2. Multiple sequence alignment of Nro1. Selected eukaryotic orthologs of Nro1 were aligned using ClustalW (Chenna et al. 2003). Strictly conserved residues are in white on a black background. Partially conserved amino acids are boxed. The apparent conservation of the C-terminal region results in part from the subset of sequences selected. Secondary structure elements assigned from the *S. pombe* Nro1$_{\Delta N54}$ structure are indicated *above* the alignment. Black stars *below* the sequences depict conserved residues near the ligand binding sites, which have been mutated in this study. This figure was generated using the Espript server (Gouet et al. 1999).

inhibition of cellular 2-oxoglutarate-dependent dioxygenases either by O_2 depletion or by incubation with the DMOG inhibitor (a 2-oxoglutarate analog), but not by mutation of Ofd1 active mutants (Lee et al. 2009).

The coupling of dioxygenase and TPR domains within a single polypeptide chain or macromolecular complexes is not unique to C-P4H. It is also observed in prolyl-3-hydroxylase 1; leprecan-like proteins 1 and 2, which are prolyl-hydroxylases also acting on collagen (Jarnum et al. 2004; Ishikawa et al. 2009); in human Asp/Asn β-hydroxylase (Korioth et al. 1994); and histone demethylases specific for H3K27me3/me2 (Cloos et al. 2008). Finally, a prolyl 4-hydroxylase modifying Skp1, a subunit of the multi-protein E3 ubiquitin ligase complex SCF, which, among several subunits, also encompasses the TPR containing protein Sgt1, has been purified from *Dictyostelium* (Kitagawa et al. 1999; van der Wel et al. 2005).

Nro1 binds SO_4^{2-} ion and an unidentified ligand via a highly conserved region

After the last step of refinement of the model using the high-resolution (2.15 Å) data set, two strong residual electron density peaks were observed in the vicinity of helix TPR^1_B. The first density was spherical and close to R101, R104, and N105 (Nro1 *S. pombe* numbering is used in this section) (Fig. 3A). As the crystals were grown in 1.6 M ammonium sulfate as a precipitant, we attributed this density to a SO_4^{2-} ion. It is noteworthy that a sulfate ion is found in the same position on the two Nro1 molecules present in the asymmetric unit. The second unexplained residual electron density peak lies at a crystal packing site. This density is planar and could accommodate an aromatic indole or purine moiety (Fig. 3A). None of the chemicals present in the purification buffer or crystallization solution seem to fit in this electron density. Hence, it is very likely that this unknown ligand originates from the *E. coli* broth and was copurified with Nro1. This molecule stacks onto G94 from helix TPR^1_B and is in the vicinity from L72, H97, E98, and R101, at a distance of 10 Å from the sulfate ion. Both ligands are mainly interacting with residues from TPR^1_B. Interestingly, with the exception of Asn^{105}, all these residues are strictly conserved within Nro1/Ett1 family, strongly supporting a role of this region in Nro1/Ett1 function (Figs. 2, 3A). Additional strictly conserved and solvent-exposed residues (Q68, D100, Y120, and L124) are surrounding this region. This area contains also highly conserved residues such as D64, I96, H117, Y147, A150, E153, and R154, and altogether, these amino acids form a large conserved patch.

As this conserved region is located close to the N terminus of the crystallized Nro1 fragment, we cannot exclude that it is partly or entirely masked by the 54 deleted residues that are predicted to adopt a TPR fold in the intact protein. To assess this possibility, we investigated through modeling whether or not this region buries this conserved region, using already known structures of TPR proteins as templates. Our model reveals that this highly conserved region located at the convex side of the N-terminal part of the helical Nro1 monomer should be fully accessible to the solvent in the full-length protein (data not shown).

In crystal structures, the visualization of fortuitously bound molecules originating from the crystallization conditions, purification buffers, or the host cell used for overexpression can improve our understanding of the function of the studied proteins (Stehlin et al. 2001). This is indeed the case for sulfate ions that very often indicate binding sites for phosphate groups either present in small molecules (e.g., ATP, GTP, FAD, NADPH, FMN, hexose-6 phosphate, ...), DNA/RNA, or phosphorylated residues (de La Sierra-Gallay et al. 2004; Graille et al. 2006; Brooks et al. 2009). We therefore suggest that the sulfate pocket is naturally occupied by a phosphate group carrying ligand. Interestingly, the overexpression of *S. pombe* Hhp1, a casein kinase I family member, results in Sre1N stabilization similarly to Ofd1 depletion or Nro1 overexpression (Lee et al. 2009), thus suggesting that phosphorylation event(s) may be involved. Considering that *S. pombe* Sre1N is hyperphosphorylated (Hughes and Espenshade 2008), we cannot exclude that Nro1 interacts with this protein, thereby contributing to its stabilization. Further experiments are in progress to identify the compound bound to Nro1 in the crystal. This could provide us with clues about the binding properties of this protein and its biochemical/biological function.

Functional analysis of Ett1 outstanding residues

To analyze the function of the most highly conserved region in the Nro1/Ett1 family that binds a sulfate ion and an uncharacterized small ligand in the crystal structure, we turned to the homologous factor from *S. cerevisiae*, Ett1. Indeed, we have shown recently that an *ETT1* deletion leads to the increase of stop codon read-through (Henri et al. 2010), thus providing a convenient quantitative assay for Ett1 activity. Mutations were introduced by site-directed mutagenesis in a plasmid encoding a tagged Ett1 version, thus allowing the comparison of the level of the mutant protein relative to the tagged wild-type factor (Fig. 3B). Importantly, the tagged protein was shown in preliminary experiments to fully complement an *ETT1* deletion (see also below). Mutations were introduced to affect the following: (1) residues involved in sulfate binding (R84A/R87A according to *S. cerevisiae* Ett1 numbering, and [R101/R104] according to *S. pombe* Nro1 numbering; for clarity, the numbering scheme for *S. pombe* Nro1 is indicated in square brackets, and the correspondence between *S. cerevisiae* Ett1 and *S. pombe* Nro1 numbering schemes can be found in Fig. 3B); (2) conserved residues surrounding the small unknown ligand detected in our structure (L60A [L72]; G77A [G94]; 80**H**EC**D**83→**A**EC**A** [97HEAD100]; 80**HE**CD83→**AA**CD [97HEAD100]); and (3) conserved residues located in the

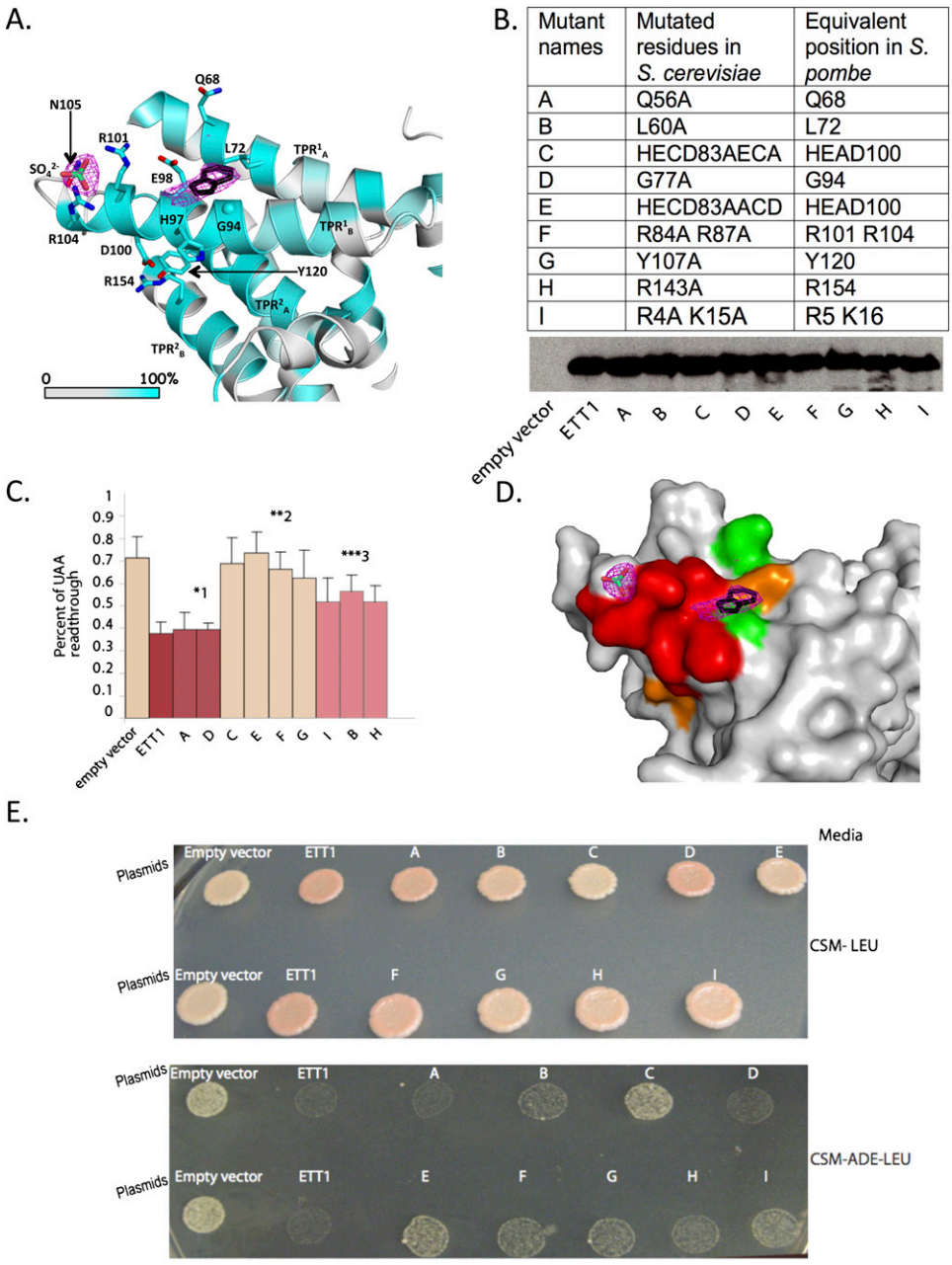

FIGURE 3. Effect of mutation of conserved Ett1 residues on stop codon read-through. (*A*) Detailed view of the ligand binding sites. Carbon atoms from Nro1$_{\Delta N54}$ residues are colored according to sequence conservation as in Figure 1C. The Cα atom from Gly^{94} is shown as a sphere. The Fo-Fc electron density map (magenta) is contoured at 3σ. The SO_4^{2-} ion originating from crystallization conditions is shown as sticks. To give an idea of the size of the residual Fo-Fc electron density close to Gly^{94}, a putative and unidentified ligand is depicted as an indole moiety by black sticks. This should not be considered as informative on the identity of the ligand. (*B*) Expression of the various mutant proteins was assayed by Western blotting through detection of the protein A tag and compared to the wild-type factor. Equal loading was ascertained by Ponceau staining. Mutants are indicated by letters with the corresponding substitutions indicated *above* the blot. (*C*) Stop codon read-through in the dual luciferase reporter. Read-through was quantified, as described in Materials and Methods, in seven independent biological replicates, each performed in technical duplicate. Standard deviations are indicated. Mutants (labeled as in *A*) were sorted in three significantly differing groups (Mann-Whitney *U*-test, 95% confidence interval): group *1 contains mutant indistinguishable from wild type, group **2 associates mutant similar to the Ett1 deletion (empty vector), while the three remaining mutants form a group (***3) with characteristics intermediate between a wild-type and an *ett1* deletion. Note that with a 99% confidence interval, the same differences were observed except that mutant B and I were then indistinguishable from the *ett1* deletion and equivalent mutants. (*D*) Mapping of the effect of the mutations on stop codon read-through at the surface of the Nro1 $_{\Delta N54}$. Mutants from groups *1, **2, and ***3 (see panel *C*) are colored green, red, and orange, respectively. Ligands and electron density are shown using the same codes as in panel *A*. (*E*) Stop codon read-through of the *ade1-14* gene was assayed both through the accumulation of the red pigment (stronger when stop codon read-through is low, compare *ETT1* and Empty vector, *upper* part) and by growth on adenine-minus media (better growth when read-through increases, *lower* part). Mutants are labeled as in panel *A*. Note that mutant labeled E is in the first row on the *top* part and in the second row on the *bottom* part. It is noteworthy that as we have previously shown that *ETT1* deletion affects stop codon read-through independently of the *PSI* phenotype (Henri et al. 2010), we did not assess the effect of guanidine chloride treatment.

vicinity of these two regions (Q56A [Q68]; Y107A [Y120]; and R143A [R154]). All these mutated residues are located in the most conserved TPR motifs (TPR^1 and TPR^2) (Fig. 2), but we also mutated into alanine conserved residues present in the first predicted TPR (TPR^0), which is absent in our structure (double mutant R4/K15 [R5/K16]).

Plasmids encoding the wild-type and mutant proteins were introduced into a strain carrying a chromosomal deletion of *ETT1*. Western blot analysis demonstrated that all proteins accumulated to similar levels, revealing that the mutation did not destabilize them (Fig. 3B). Reporter plasmids encoding two luciferases (Renilla and Firefly) separated either by a UAA stop codon or by CAA glutamine codon were then introduced with the wild-type and mutant *ETT1* to test their effect on translation termination, as previously reported (Keeling et al. 2006; Henri et al. 2010). A strain carrying the empty vector (instead of *ETT1*) was used as negative control. Read-through of the stop codon was expressed as the ratio of the Firefly luciferase determined for the UAA containing vector to the CAA encoding vector, normalized for expression of the Renilla luciferase. Consistent with our previous work, the deletion of the gene *ETT1* leads to increased stop codon read-through that is restored to a wild-type level by introduction of plasmid encoding *ETT1* (Fig. 3C,D). Statistical analysis of the results obtained with the different mutants demonstrated that those could be grouped in three distinct sets. Mutants Q56A and G77A were indistinguishable from wild type (Fig. 3C,D). In contrast, mutants 80**H**EC**D**83→**A**EC**A**, 80**HE**CD83→**AA**CD, and R84A/R87A located in the $TPR^1{}_B$ and Y107A located in the $TPR^2{}_A$ increased stop codon read-through in the same way as the *ett1* null mutant. Finally, R4A/K15A, L60A, and R143A localized respectively in the N-terminal region of the Ett1, $TPR^1{}_A$, and $TPR^2{}_B$ helices have an intermediate effect on read-through, suggesting that they are only partially functional (Fig. 3C,D).

To validate these results and further demonstrate that the read-through effect is not specific for the UAA stop codon, we assayed for the expression of the *ADE1* gene (Fig. 3E). Indeed, the strain carries an *ade1-14* mutation resulting from the presence of a premature UGA stop codon (Keeling et al. 2006). In the presence of the wild-type *ETT1* gene, the resulting strain displays a red color (upper panel) and is unable to grow on media lacking adenine (lower panel). When *ETT1* is inactivated, read-through of the UGA stop codon allows the strain to grow in the absence of adenine, and the strain appears white. Despite the lower sensitivity of this second assay, the results obtained agree closely with those obtained with the reporter plasmid (Fig. 3, cf. C and E). This indicates that the phenotypes observed result indeed from a general increase of stop codon read-through, and reinforces the conclusions concerning the functionality of the various *ETT1* mutants.

The inactivity of the mutant R84A/R87A shows that the integrity of the sulfate binding pocket is important for Ett1 function. The observation that the substitution of HE at positions 80 and 81 by alanines (mutant 80**HE**CD83→**AA**CD) mimics the *ett1Δ* mutant suggests that binding of the unidentified ligand by Ett1 is also functionally relevant. This interpretation is further supported by the fact that mutation of another residue surrounding this ligand, namely, L60, also partly abolishes Ett1 function. Surprisingly, however, mutation of G77, another residue close to the ligand does not impair Ett1 activity. This can suggest either that the substitution of G77 by an alanine is not sufficient to disrupt the interaction with the ligand or, alternatively, that the active form of Ett1 is unliganded. Further evidence for the crucial role of this region comes from the observation that both the 80**H**EC**D**83→**A**EC**A** and Y107A mutations also completely abolish Ett1 function. However, this area is not the only one implicated in Ett1 activity, as mutation of other residues such as R143 located in $TPR^2{}_B$ or R4A/K15A located in the N-terminal region missing in the crystallized protein also partially inactivate Ett1. Not all conserved residues are critical, as mutations of the absolutely conserved G77 (see above) or Q56 result in Ett1 variants indistinguishable from the wild-type factor. In summary, this extensive site-directed mutagenesis approach clearly shows that most of the strictly conserved residues involved in binding of the sulfate ion and of the ligand, whose identity remains to be determined, are crucial for Ett1 activity on translation termination accuracy (Fig. 3A,D).

CONCLUSIONS

In conclusion, the crystal structure of *S. pombe* Nro1 reveals that it is a TPR protein, despite being a noncanonical member of this family. The structure highlights a highly conserved region that binds sulfate and an unidentified molecule, while functional assays demonstrate the importance of these key residues. Many structures of TPR domains have been solved to date, but given that such modules are implicated in widespread biological activities, this does not suggest an Nro1/Ett1 function beyond a role in protein interaction. Although we have now described their crystal structures and identified functional residues implicated in optimal stop codon recognition, the precise role of Tpa1/Ofd1 and Nro1/Ett1 in the control of translation termination accuracy or the O_2-dependent regulation of Sre1 stability remains to be clarified at the molecular level. In particular, we will focus our attention on the identification of the ligand bound to *S. pombe* Nro1. Further studies will also be needed to clarify the interconnection between Nro1/Ett1 and Tpa1/Ofd1 and to identify the mechanistic differences that allow Nro1, but not Ett1, to inhibit Ofd1/Tpa1 activity. Interestingly, while Tpa1/Ofd1 has a clear human ortholog, this is not the case for Nro1/Ett1. The biological reasons supporting this difference will also need to be investigated.

MATERIALS AND METHODS

Cloning, expression, and purification

A DNA sequence was designed to encode *S. pombe* Ofd1 (without tag) and Nro1 deleted from its 54 N-terminal residues ($Nro1_{\Delta N54}$ and fused to a N-terminal hexahistidine tag) proteins. This fragment was obtained by de novo gene synthesis (GenScript Corporation) and was further subcloned into pET21-a between the NcoI and XhoI sites. The proteins were expressed using *E. coli* Rosetta pLysS strain at 23°C in 2×YT medium supplemented with ampicillin (50 μg/mL) and chloramphenicol (25 μg/mL). At OD_{600} = 0.8, transcription of the recombinant operon was induced by the addition of 50 μg/mL IPTG for 20 h. Cells were harvested by centrifugation; resuspended in 25 mL of 20 mM Tris-HCl (pH 7.5), 200 mM NaCl, and 5 mM β-mercaptoethanol (buffer A); and stored at −20°C. Cell lysis was performed by sonication. The lysate was incubated with DNases/RNases (20 μg/mL; Sigma) and centrifuged (30 min at 20,000 rpm). The supernatant was applied onto an Ni-NTA column (Qiagen). Following elution at 100 mM imidazole, enrichment in two proteins that migrated to the expected molecular weight for $Nro1_{\Delta N54}$ and Ofd1 was observed on SDS/PAGE. Next, a gel filtration chromatography on a Superdex 200 HL 16/60 column (GE Healthcare) equilibrated in buffer A was performed. During this step, the two proteins migrating at the molecular weight expected for $Nro1_{\Delta N54}$ and Ofd1 exhibited different elution volumes, allowing their separation. Two successive anion exchange chromatographic steps on a HiTrap Q FF column (GE Healthcare) with different NaCl salt gradients were applied, and the $Nro1_{\Delta N54}$ protein, eluted at 400 mM NaCl, was dialyzed against buffer A. Protein Se-Met labeling was conducted using standard routines (Hendrickson et al. 1990), and the labeled protein was purified using the same protocol as the native protein.

Structure determination

Crystals of the native protein (form I) were grown from a mixture in a 1:1 ratio of 7.2 mg/mL protein solution in buffer A and crystallization liquor containing 0.1M Hepes (pH 7.0), 1.6 M ammonium sulfate, and 10 mM $MgCl_2$, in 2 μL hanging drops. Crystals of the SeMet protein (Form II) were grown in the same conditions except for the addition of 3% polyvinylpyrrolidone, in 1 μL sitting drops. The crystals were cryo-protected by transfer into the crystallization condition with progressively higher ethylene glycol concentration up to 30% and then flash-cooled in liquid nitrogen.

Crystal form I yielded diffraction up to 3.5 Å resolution on beam line Proxima-1 at SOLEIL synchrotron. This crystal belongs to space group $P6_522$ with one molecule in the asymmetric unit. Crystal form II diffracted up to 2.15 Å resolution, but the high-resolution limit decreased with time. This crystal belongs to space group $P2_1$ with two molecules in the asymmetric unit (a = 48.9Å, b = 107.8Å, c = 101.8Å, β = 102.3°).

The structure was determined from Se-Met–labeled protein crystals by the multi-wavelength anomalous dispersion method using the anomalous signal of selenium atoms. Data were processed with the XDS package (Kabsch 1993). Considering the cell parameters and the molecular mass of the protein, the Matthews coefficient suggested that two molecules and 70% of the solvent were present in the asymmetric unit. The program SHELXD was used to locate the six expected Se sites (three per molecule) (Schneider and Sheldrick 2002). Refinement of these Se sites and phasing were carried out with the program SHARP (Bricogne et al. 2003). The obtained experimental electron density map was of excellent quality and allowed automatic building by ARP-WARP. Iterative cycles of manual rebuilding using COOT (Emsley and Cowtan 2004) followed by refinement with PHENIX (Adams et al. 2002) led to an almost complete model containing two Nro1 molecules, 567 water molecules, 2 Cl^- ions, three ethylene glycol molecules, and two SO_4^{2-} ions in the asymmetric unit. The loop between Asn^{303} and Val^{308} could not be built due to lack of electron density. Analysis of the 2Fo-Fc electron density map revealed that Cys258 from both monomers are present as β-mercaptoethanol derivatives. All the residues from each monomer display main chain dihedral angles that fall within allowed regions of the Ramachandran plot.

This model was then used for molecular replacement with MOLREP (Vagin and Teplyakov 1997) using the native low resolution data set and finally submitted to a new series of manual rebuilding with COOT and refinement with PHENIX. This allowed us to build the N-terminal His_6-tag and the Asn^{303}-Val^{308} loop, thereby leading to a complete model of the crystallized protein. The statistics for data collection and refinement are summarized in Table 1. The atomic coordinates and structure factors have been deposited into the Brookhaven Protein Data Bank under accession numbers (3QTM and 3QTN for the models refined against high- and low-resolution data, respectively).

Strains and media

The *S. cerevisiae* strain BSY2236 (*MATa leu2-3,112 his3-11,15 trp1-1 ura3-1 ade1-14 ett1::HIS3* [PSI^+]) is a derivative of YJW618 carrying a HIS3-marked deletion of *ETT1* (Henri et al. 2010). YJW618 was a kind gift from D.M. Bedwell (Keeling et al. 2006). Cells were grown at 30°C in standard media.

The plasmid pBS3972, containing the wild-type *ETT1* gene, was constructed by amplifying the *ETT1* ORF with upstream and downstream sequences from genomic DNA using OBS4227 and OBS4228 and inserting the resulting fragment between the BamHI and XhoI sites of the pRS425 (*LEU2*, 2μ) vector (Christianson et al. 1992). The sequence encoding the TAP tag was then fused to the C-terminal end of the *ETT1* coding sequence by a PCR and cloning using oligonucleotides OBS4283-OBS4286, yielding plasmid pBS3973. Mutant alleles were constructed by site-directed mutagenesis of pBS3973 with primers OBS4287-OBS4306 by amplification of the whole plasmid and digestion of the parental DNA with DpnI. Oligonucleotides and plasmids are described in detail in Supplemental Tables 1 and 2.

Stop codon read-through measurements

Reporters encoding the Renilla and Firefly luciferases separated either by a stop codon (UAA) or by a sense codon (CAA) (Keeling et al. 2006) were introduced in yeast cells by transformation (Ito et al. 1983). Pools of three transformants were grown in selective liquid media to OD_{600} 0.5–0.8. Ten microliters of yeast culture was used for enzymatic assays using the dual luciferase reporter assay reagent (Promega). Luminescence was quantified in a Berthold luminometer. The percentage of read-through is the ratio of Firefly luciferase produced by the stop codon containing construct to the Firefly luciferase CAA containing construct, normalized, to the level of Renilla luciferase produced in the same cells. Seven biological

TABLE 1. Statistics for data collection and refinement

	Form I	Form II			
		MAD			
		Peak	Inflexion	Remote	High resolution
Wavelength (Å)	0.98	0.9791	0.97946	0.95373	0.979
Space group	$P6_522$	$P2_1$			
Cell parameters	a = b = 124.1 Å; c = 205.5 Å	a = 48.9 Å; b = 107.8 Å; c = 101.8 Å; β = 102.3°			
Resolution (Å)	25–3.5 (3.7–3.5)	45–2.3 (2.4–2.3)	45–2.9 (3.1–2.9)	45–3.0 (3.2–3)	40–2.15 (2.3–2.15)
Total no. of reflections	46,371	341,057	138,226	138,886	227,506
Total no. of unique reflections	11,950	91,031	44,142	40,401	108,245
R_{sym} (%)[a]	11.3 (57.8)	12.7 (60.9)	11.1 (64)	14.8 (62.2)	8.9 (46.7)
Completeness (%)	97.3 (98.9)	98.2 (89.5)	99.1 (97)	98.4 (92.2)	97.4 (86.8)
I/σ(I)	11.3 (2.4)	8.7 (2.44)	9.8 (2)	8.4 (2.4)	6.3 (1.7)
Redundancy	3.9	3.75	3.1	3.4	2.1
Refinement					
Resolution (Å)	25–3.5				40–2.15
R/R_{free} (%)[b]	19.4/25.4				17.8/21.3
rmsd bonds (Å)	0.008				0.007
rmsd angles (°)	1.118				0.91

Values in parentheses are for the highest-resolution shell.
[a]$R_{sym} = \Sigma_h\Sigma_i|I_{hi} - \langle I_h\rangle|/\Sigma_h\Sigma_i I_{hi}$, where I_{hi} is the *i*th observation of the reflection h, while $\langle I_h\rangle$ is the mean intensity of reflection h.
[b]$R_{factor} = \Sigma\ ||F_o| - |F_c||/|F_o|$. R_{free} was calculated with a small fraction (5%) of randomly selected reflections.

experiments were performed with, in each case, technical duplicates. The Mann-Whitney *U*-test was used to test the significance of such observations as previously (Keeling et al. 2006, Henri et al. 2010). Indeed, this test is not dependent upon a normal distribution of the values assayed.

For monitoring the suppression of the UGA codon present in *ade1* (ade1-14 allele), 5 µL of yeast culture at OD around 0,1 was deposited on two selective plates without leucine for the color assay and without adenine and leucine for the growth assay. Plates were incubated at 30°C during 3 d. For the color assay, cells were transferred at 4°C for at least one night before being photographed.

Protein analyses

Proteins extracted from yeast using a rapid protocol (Kushnirov 2000) were fractionated on 8% SDS PAGE and blotted to nitrocellulose. TAP tagged proteins were decorated with PAP (Sigma) and detected using an ECL kit (GE Healthcare).

SUPPLEMENTAL MATERIAL

Supplemental material is available for this article.

ACKNOWLEDGMENTS

We thank K. Blondeau for her help with SeMet labeling, V. Heurgué-Hamard for anti-eRF1 antibodies, D.M. Bedwell (University of Alabama, Birmingham) for providing YJW618, and A. Doizy and B. Bonneau for technical assistance. We thank M. Argentini and D. Cornu for mass spectrometry analysis (SICaps, IMAGIF platform, Gif/Yvette, France) and the IGBMC (Institut de Génétique et de Biologie Moléculaire et Cellulaire) for assistance. This work was supported by the CNRS, the European Union Sixth Framework program "3D-Repertoire" (LSHG-CT-2005-512028) to H.v.T. and B.S., the Ligue Contre le Cancer (Equipe Labellisée 2011) to B.S., and the Agence Nationale pour la Recherche (Grant ANR-06-BLAN-0075-02) to M.G. and (Grant ANR-07-BLAN-0093) to B.S. J.H. is a recipient of a Ph.D. fellowship from Université Paris Sud-11. D.R. was supported by a fellowship from Université Paris Sud-11 and then by the Fondation pour la Recherche Médicale (FRM). We thank SOLEIL for provision of synchrotron radiation facilities, and we thank Andrew Thompson and Pierre Legrand for assistance with beamline Proxima-1.

NOTE ADDED IN PROOF

While this article was being edited, the crystal structure at 2.2 Å resolution of full-length *S. Pombe* Nro1 protein was reported (Yeh et al. 2011). The full-length protein crystallized in the same space group as our truncated form, resulting in a low rmsd between both structures (rmsd of 0.4 A over 328 Ca atoms). In the full-length structure, part (residues 4–19) of the N-terminal region, absent in our study, is visible and folds as an α-helix. However, it cannot be considered as a TPR motif contrary to our prediction based on a bioinformatics analysis. Yeh et al. present data supporting a role of Nro1 in nuclear import and suggesting that residues 4–19 of Nro1 are interacting with Ofd1.

Received February 25, 2011; accepted April 1, 2011.

REFERENCES

Adams PD, Grosse-Kunstleve RW, Hung LW, Ioerger TR, McCoy AJ, Moriarty NW, Read RJ, Sacchettini JC, Sauter NK, Terwilliger TC. 2002. PHENIX: building new software for automated crystallographic structure determination. *Acta Crystallogr D Biol Crystallogr* **58:** 1948–1954.

Alcazar-Roman AR, Bolger TA, Wente SR. 2010. Control of mRNA export and translation termination by inositol hexakisphosphate requires specific interaction with Gle1. *J Biol Chem* **285:** 16683–16692.

Alkalaeva EZ, Pisarev AV, Frolova LY, Kisselev LL, Pestova TV. 2006. In vitro reconstitution of eukaryotic translation reveals cooperativity between release factors eRF1 and eRF3. *Cell* **125:** 1125–1136.

Balagopal V, Parker R. 2009. Stm1 modulates mRNA decay and Dhh1 function in *Saccharomyces cerevisiae*. *Genetics* **181:** 93–103.

Bolger TA, Folkmann AW, Tran EJ, Wente SR. 2008. The mRNA export factor Gle1 and inositol hexakisphosphate regulate distinct stages of translation. *Cell* **134:** 624–633.

Bonetti B, Fu L, Moon J, Bedwell DM. 1995. The efficiency of translation termination is determined by a synergistic interplay between upstream and downstream sequences in *Saccharomyces cerevisiae*. *J Mol Biol* **251:** 334–345.

Bricogne G, Vonrhein C, Flensburg C, Schiltz M, Paciorek W. 2003. Generation, representation and flow of phase information in structure determination: recent developments in and around SHARP 2.0. *Acta Crystallogr D Biol Crystallogr* **59:** 2023–2030.

Brooks MA, Dziembowski A, Quevillon-Cheruel S, Henriot V, Faux C, van Tilbeurgh H, Seraphin B. 2009. Structure of the yeast Pml1 splicing factor and its integration into the RES complex. *Nucleic Acids Res* **37:** 129–143.

Carr-Schmid A, Pfund C, Craig EA, Kinzy TG. 2002. Novel G-protein complex whose requirement is linked to the translational status of the cell. *Mol Cell Biol* **22:** 2564–2574.

Chen XQ, Du X, Liu J, Balasubramanian MK, Balasundaram D. 2004. Identification of genes encoding putative nucleoporins and transport factors in the fission yeast *Schizosaccharomyces pombe*: a deletion analysis. *Yeast* **21:** 495–509.

Chen L, Muhlrad D, Hauryliuk V, Cheng Z, Lim MK, Shyp V, Parker R, Song H. 2010. Structure of the Dom34-Hbs1 complex and implications for no-go decay. *Nat Struct Mol Biol* **17:** 1233–1240.

Cheng Z, Saito K, Pisarev AV, Wada M, Pisareva VP, Pestova TV, Gajda M, Round A, Kong C, Lim M, et al. 2009. Structural insights into eRF3 and stop codon recognition by eRF1. *Genes Dev* **23:** 1106–1118.

Chenna R, Sugawara H, Koike T, Lopez R, Gibson TJ, Higgins DG, Thompson JD. 2003. Multiple sequence alignment with the Clustal series of programs. *Nucleic Acids Res* **31:** 3497–3500.

Christianson TW, Sikorski RS, Dante M, Shero JH, Hieter P. 1992. Multifunctional yeast high-copy-number shuttle vectors. *Gene* **110:** 119–122.

Cloos PA, Christensen J, Agger K, Helin K. 2008. Erasing the methyl mark: histone demethylases at the center of cellular differentiation and disease. *Genes Dev* **22:** 1115–1140.

Cole SE, LaRiviere FJ, Merrikh CN, Moore MJ. 2009. A convergence of rRNA and mRNA quality control pathways revealed by mechanistic analysis of nonfunctional rRNA decay. *Mol Cell* **34:** 440–450.

Cosson B, Couturier A, Chabelskaya S, Kiktev D, Inge-Vechtomov S, Philippe M, Zhouravleva G. 2002. Poly(A)-binding protein acts in translation termination via eukaryotic release factor 3 interaction and does not influence [PSI$^+$] propagation. *Mol Cell Biol* **22:** 3301–3315.

D'Andrea LD, Regan L. 2003. TPR proteins: the versatile helix. *Trends Biochem Sci* **28:** 655–662.

de La Sierra-Gallay IL, Collinet B, Graille M, Quevillon-Cheruel S, Liger D, Minard P, Blondeau K, Henckes G, Aufrère R, Leulliot N, et al. 2004. Crystal structure of the YGR205w protein from *Saccharomyces cerevisiae*: close structural resemblance to *E. coli* pantothenate kinase. *Proteins* **54:** 776–783.

Doma MK, Parker R. 2006. Endonucleolytic cleavage of eukaryotic mRNAs with stalls in translation elongation. *Nature* **440:** 561–564.

Doma MK, Parker R. 2007. RNA quality control in eukaryotes. *Cell* **131:** 660–668.

Emsley P, Cowtan K. 2004. Coot: model-building tools for molecular graphics. *Acta Crystallogr D Biol Crystallogr* **60**(Pt 12 Pt 1): 2126–2132.

Estrella LA, Wilkinson MF, Gonzalez CI. 2009. The shuttling protein Npl3 promotes translation termination accuracy in *Saccharomyces cerevisiae*. *J Mol Biol* **394:** 410–422.

Frolova LY, Tsivkovskii RY, Sivolobova GF, Oparina NY, Serpinsky OI, Blinov VM, Tatkov SI, Kisselev LL. 1999. Mutations in the highly conserved GGQ motif of class 1 polypeptide release factors abolish ability of human eRF1 to trigger peptidyl-tRNA hydrolysis. *RNA* **5:** 1014–1020.

Frolova L, Seit-Nebi A, Kisselev L. 2002. Highly conserved NIKS tetrapeptide is functionally essential in eukaryotic translation termination factor eRF1. *RNA* **8:** 129–136.

Gouet P, Courcelle E, Stuart DI, Metoz F. 1999. ESPript: analysis of multiple sequence alignments in PostScript. *Bioinformatics* **15:** 305–308.

Graille M, Baltaze JP, Leulliot N, Liger D, Quevillon-Cheruel S, van Tilbeurgh H. 2006. Structure-based functional annotation: yeast ymr099c codes for a D-hexose-6-phosphate mutarotase. *J Biol Chem* **281:** 30175–30185.

Graille M, Chaillet M, van Tilbeurgh H. 2008. Structure of yeast Dom34: a protein related to translation termination factor Erf1 and involved in No-Go decay. *J Biol Chem* **283:** 7145–7154.

Gross T, Siepmann A, Sturm D, Windgassen M, Scarcelli JJ, Seedorf M, Cole CN, Krebber H. 2007. The DEAD-box RNA helicase Dbp5 functions in translation termination. *Science* **315:** 646–649.

Hendrickson WA, Horton JR, LeMaster DM. 1990. Selenomethionyl proteins produced for analysis by multiwavelength anomalous diffraction (MAD): a vehicle for direct determination of three-dimensional structure. *EMBO J* **9:** 1665–1672.

Henri J, Rispal D, Bayart E, van Tilbeurgh H, Seraphin B, Graille M. 2010. Structural and functional insights into *Saccharomyces cerevisiae* Tpa1, a putative prolylhydroxylase influencing translation termination and transcription. *J Biol Chem* **285:** 30767–30778.

Hieta R, Kukkola L, Permi P, Pirila P, Kivirikko KI, Kilpelainen I, Myllyharju J. 2003. The peptide-substrate-binding domain of human collagen prolyl 4-hydroxylases. Backbone assignments, secondary structure, and binding of proline-rich peptides. *J Biol Chem* **278:** 34966–34974.

Holm L, Kaariainen S, Rosenstrom P, Schenkel A. 2008. Searching protein structure databases with DaliLite v.3. *Bioinformatics* **24:** 2780–2781.

Hughes BT, Espenshade PJ. 2008. Oxygen-regulated degradation of fission yeast SREBP by Ofd1, a prolyl hydroxylase family member. *EMBO J* **27:** 1491–1501.

Hughes AL, Todd BL, Espenshade PJ. 2005. SREBP pathway responds to sterols and functions as an oxygen sensor in fission yeast. *Cell* **120:** 831–842.

Hughes AL, Lee CY, Bien CM, Espenshade PJ. 2007. 4-Methyl sterols regulate fission yeast SREBP-Scap under low oxygen and cell stress. *J Biol Chem* **282:** 24388–24396.

Ishikawa Y, Wirz J, Vranka JA, Nagata K, Bachinger HP. 2009. Biochemical characterization of the prolyl 3-hydroxylase 1.cartilage-associated protein.cyclophilin B complex. *J Biol Chem* **284:** 17641–17647.

Ito H, Fukuda Y, Murata K, Kimura A. 1983. Transformation of intact yeast cells treated with alkali cations. *J Bacteriol* **153:** 163–168.

Jarnum S, Kjellman C, Darabi A, Nilsson I, Edvardsen K, Aman P. 2004. LEPREL1, a novel ER and Golgi resident member of the Leprecan family. *Biochem Biophys Res Commun* **317:** 342–351.

Kabsch W. 1993. Automatic processing of rotation diffraction data from crystals of initially unknown symmetry and cell constants. *J Appl Crystallogr* **26:** 795–800.

Keeling KM, Salas-Marco J, Osherovich LZ, Bedwell DM. 2006. Tpa1p is part of an mRNP complex that influences translation termination, mRNA deadenylation, and mRNA turnover in *Saccharomyces cerevisiae*. *Mol Cell Biol* **26:** 5237–5248.

Khoshnevis S, Gross T, Rotte C, Baierlein C, Ficner R, Krebber H. 2010. The iron-sulphur protein RNase L inhibitor functions in translation termination. *EMBO Rep* **11:** 214–219.

Kim K, Oh J, Han D, Kim EE, Lee B, Kim Y. 2006. Crystal structure of PilF: functional implication in the type 4 pilus biogenesis in *Pseudomonas aeruginosa*. *Biochem Biophys Res Commun* **340:** 1028–1038.

Kim HS, Kim HL, Kim KH, Kim DJ, Lee SJ, Yoon JY, Yoon HJ, Lee HY, Park SB, Kim SJ, et al. 2010. Crystal structure of Tpa1 from *Saccharomyces cerevisiae*, a component of the messenger ribonucleoprotein complex. *Nucleic Acids Res* **38:** 2099–2110.

Kitagawa K, Skowyra D, Elledge SJ, Harper JW, Hieter P. 1999. SGT1 encodes an essential component of the yeast kinetochore assembly pathway and a novel subunit of the SCF ubiquitin ligase complex. *Mol Cell* **4:** 21–33.

Kobayashi K, Kikuno I, Kuroha K, Saito K, Ito K, Ishitani R, Inada T, Nureki O. 2010. Structural basis for mRNA surveillance by archaeal Pelota and GTP-bound EF1α complex. *Proc Natl Acad Sci* **107:** 17575–17579.

Kong C, Ito K, Walsh MA, Wada M, Liu Y, Kumar S, Barford D, Nakamura Y, Song H. 2004. Crystal structure and functional analysis of the eukaryotic class II release factor eRF3 from S. pombe. *Mol Cell* **14:** 233–245.

Korioth F, Gieffers C, Frey J. 1994. Cloning and characterization of the human gene encoding aspartyl β-hydroxylase. *Gene* **150:** 395–399.

Krogan NJ, Cagney G, Yu H, Zhong G, Guo X, Ignatchenko A, Li J, Pu S, Datta N, Tikuisis AP, et al. 2006. Global landscape of protein complexes in the yeast *Saccharomyces cerevisiae*. *Nature* **440:** 637–643.

Kushner DB, Lindenbach BD, Grdzelishvili VZ, Noueiry AO, Paul SM, Ahlquist P. 2003. Systematic, genome-wide identification of host genes affecting replication of a positive-strand RNA virus. *Proc Natl Acad Sci* **100:** 15764–15769.

Kushnirov VV. 2000. Rapid and reliable protein extraction from yeast. *Yeast* **16:** 857–860.

Lee CY, Stewart EV, Hughes BT, Espenshade PJ. 2009. Oxygen-dependent binding of Nro1 to the prolyl hydroxylase Ofd1 regulates SREBP degradation in yeast. *EMBO J* **28:** 135–143.

Nissen P, Kjeldgaard M, Thirup S, Polekhina G, Reshetnikova L, Clark BF, Nyborg J. 1995. Crystal structure of the ternary complex of Phe-tRNAPhe, EF-Tu, and a GTP analog. *Science* **270:** 1464–1472.

Pekkala M, Hieta R, Bergmann U, Kivirikko KI, Wierenga RK, Myllyharju J. 2004. The peptide-substrate-binding domain of collagen prolyl 4-hydroxylases is a tetratricopeptide repeat domain with functional aromatic residues. *J Biol Chem* **279:** 52255–52261.

Rice LM, Brunger AT. 1999. Crystal structure of the vesicular transport protein Sec17: implications for SNAP function in SNARE complex disassembly. *Mol Cell* **4:** 85–95.

Riggs DL, Roberts PJ, Chirillo SC, Cheung-Flynn J, Prapapanich V, Ratajczak T, Gaber R, Picard D, Smith DF. 2003. The Hsp90-binding peptidylprolyl isomerase FKBP52 potentiates glucocorticoid signaling in vivo. *EMBO J* **22:** 1158–1167.

Rout MP, Aitchison JD, Suprapto A, Hjertaas K, Zhao Y, Chait BT. 2000. The yeast nuclear pore complex: composition, architecture, and transport mechanism. *J Cell Biol* **148:** 635–651.

Schneider TR, Sheldrick GM. 2002. Substructure solution with SHELXD. *Acta Crystallogr D Biol Crystallogr* **58**(Pt 10 Pt 2): 1772–1779.

Shoemaker CJ, Eyler DE, Green R. 2010. Dom34:Hbs1 promotes subunit dissociation and peptidyl-tRNA drop-off to initiate no-go decay. *Science* **330:** 369–372.

Song H, Mugnier P, Das AK, Webb HM, Evans DR, Tuite MF, Hemmings BA, Barford D. 2000. The crystal structure of human eukaryotic release factor eRF1–mechanism of stop codon recognition and peptidyl-tRNA hydrolysis. *Cell* **100:** 311–321.

Stehlin C, Wurtz JM, Steinmetz A, Greiner E, Schule R, Moras D, Renaud JP. 2001. X-ray structure of the orphan nuclear receptor RORβ ligand-binding domain in the active conformation. *EMBO J* **20:** 5822–5831.

Taylor DJ, Frank J, Kinzy TG. 2007. Structure and function of the eukaryotic ribosome and elongation factors. In *Translational control in biology and medicine* (ed. MB Mathews et al.), Vol. 1, pp. 59–86. Cold Spring Harbor Laboratory Press, Cold Spring Harbor, NY.

Todd BL, Stewart EV, Burg JS, Hughes AL, Espenshade PJ. 2006. Sterol regulatory element binding protein is a principal regulator of anaerobic gene expression in fission yeast. *Mol Cell Biol* **26:** 2817–2831.

Vagin A, Teplyakov A. 1997. MOLREP: an automated program for molecular replacement. *J Appl Crystallogr* **30:** 1022–1025.

van den Elzen AM, Henri J, Lazar N, Gas ME, Durand D, Lacroute F, Nicaise M, van Tilbeurgh H, Seraphin B, Graille M. 2010. Dissection of Dom34-Hbs1 reveals independent functions in two RNA quality control pathways. *Nat Struct Mol Biol* **17:** 1446–1452.

van der Wel H, Ercan A, West CM. 2005. The Skp1 prolyl hydroxylase from Dictyostelium is related to the hypoxia-inducible factor-α class of animal prolyl 4-hydroxylases. *J Biol Chem* **280:** 14645–14655.

Van Dyke MW, Nelson LD, Weilbaecher RG, Mehta DV. 2004. Stm1p, a G4 quadruplex and purine motif triplex nucleic acid-binding protein, interacts with ribosomes and subtelomeric Y′ DNA in *Saccharomyces cerevisiae*. *J Biol Chem* **279:** 24323–24333.

Wu B, Li P, Liu Y, Lou Z, Ding Y, Shu C, Ye S, Bartlam M, Shen B, Rao Z. 2004. 3D structure of human FK506-binding protein 52: implications for the assembly of the glucocorticoid receptor/Hsp90/immunophilin heterocomplex. *Proc Natl Acad Sci* **101:** 8348–8353.

Yeh TL, Lee CYS, Amzel LM, Espenshade PJ, Bianchet MA. 2011. The hypoxic regulator of sterol synthesis Nro1 is a nuclear import adaptor. *Structure* **19:** 503–514.

Zhouravleva G, Frolova L, Le Goff X, Le Guellec R, Inge-Vechtomov S, Kisselev L, Philippe M. 1995. Termination of translation in eukaryotes is governed by two interacting polypeptide chain release factors, eRF1 and eRF3. *EMBO J* **14:** 4065–4072.